VIP Metal-Organic Frameworks Very Important Paper

How to cite: *Angew. Chem. Int. Ed.* **2020**, *59*, 22749–22755
International Edition: doi.org/10.1002/anie.202011614
German Edition: doi.org/10.1002/ange.202011614

Incorporating Transition-Metal Phosphides Into Metal-Organic Frameworks for Enhanced Photocatalysis

*Kang Sun, Meng Liu, Junzhe Pei, Dandan Li, Chunmei Ding, Kaifeng Wu, and Hai-Long Jiang**

Abstract: *Metal-organic frameworks (MOFs) have been shown to be an excellent platform in photocatalysis. However, to suppress electron–hole recombination, a Pt cocatalyst is usually inevitable, especially in photocatalytic H_2 production, which greatly limits practical application. Herein, for the first time, monodisperse, small-size, and noble-metal-free transitional-metal phosphides (TMPs; for example, Ni_2P, $Ni_{12}P_5$), are incorporated into a representative MOF, UiO-66-NH_2, for photocatalytic H_2 production. Compared with the parent MOF and their physical mixture, both TMPs@MOF composites display significantly improved H_2 production rates. Thermodynamic and kinetic studies reveal that TMPs, behaving similar ability to Pt, greatly accelerate the linker-to-cluster charge transfer, promote charge separation, and reduce the activation energy of H_2 production. Significantly, the results indicate that Pt is thermodynamically favorable, yet Ni_2P is kinetically preferred for H_2 production, accounting for the higher activity of Ni_2P@UiO-66-NH_2 than Pt@UiO-66-NH_2.*

Introduction

With the rapid depletion of conventional energy sources and associated environmental issues, increasing renewable energy demand is being intensively pursued. The conversion of solar energy to chemical energy or high valued chemicals, by means of photocatalysis, has been recognized to be an attractive solution and intensively studied.[1] Amongst diverse photocatalytic processes, photocatalytic water splitting to generate H_2, an ideal and very promising future fuel, is being the most studied reaction. However, the currently reported photocatalysts toward this conversion suffer from severe photogenerated electron-hole (e-h) recombination, insufficient reaction sites, and low efficiency, posing significant challenge for further practical application.[2] The most urgent task along this research line is to develop suitable photocatalytic systems with efficient photocatalysts greatly promoting charge separation toward hydrogen production.

The introduction of cocatalyst has been well established to be the most effective way to suppress the charge recombination, provide adequate active sites and reduce activation energy for H_2 evolution.[3] Noble metals (e.g. Pt) are well-known as the most used and efficient cocatalysts. However, their high-cost and limited-reserves drive the demand to explore non-precious metal cocatalysts with low cost and high efficiency. Transition-metal phosphides (TMPs), such as Ni_2P, $Ni_{12}P_5$, Co_2P, etc., have been recently reported as promising noble-metal-alternative cocatalysts toward photocatalytic hydrogen production due to their unique structural and electronic properties.[4–6] Despite significant progress on this aspect, two challenging issues arise out of those previous reports: 1) The activity comparison between TMPs and Pt remains a topic of debate. Some reports suggest that H_2 production rate of the TMP cocatalysts is even higher than Pt,[4b,e,6c] whereas some other studies believe that the TMP activity is lower than Pt.[4a,d,6b] The former explains this phenomenon based on the kinetic results, while the latter explains it from the perspective of electrochemistry by comparing the on-set overpotential in the polarization curves, in which the on-set overpotential of Pt is lower than that of TMPs. Therefore, the current interpretation and understanding on TMP cocatalyst might be one-sided, and further in-depth study and complete understanding are highly desired. 2) The large particle sizes of TMPs and small interface contact with semiconductors. Although some nanostructured TMPs have been synthesized via the surfactant-assisted strategy, their high surface energy gives rise to a strong tendency to agglomeration during the reaction.[3b] Most of TMPs in previous reports were prepared from the precursors of metal salts, oxides, etc.,[4b,d,e,6b,c] where the resultant large particle sizes of TMPs cause very limited interface contact, or even in a physical mixture form, between TMPs and semiconductors, detrimental to photocatalysis.

In addition to cocatalyst, the development of optimized photocatalyst is of great importance for improving charge separation. In contrast to the traditional solid semiconductors, porous materials feature high porosity and high surface area, not only favorable to the dispersion and accessibility of cocatalysts but also beneficial to the transport of substrates and products.[7] Moreover, they enable charge carriers short-

[*] K. Sun, J. Pei, Prof. Dr. H.-L. Jiang
Hefei National Laboratory for Physical Sciences at the Microscale, CAS Key Laboratory of Soft Matter Chemistry, Department of Chemistry, University of Science and Technology of China
Hefei, Anhui 230026 (P. R. China)
E-mail: jianglab@ustc.edu.cn

M. Liu, Prof. Dr. K. Wu
State Key Laboratory of Molecular Reaction Dynamics, Dalian Institute of Chemical Physics, Chinese Academy of Sciences
Dalian, Liaoning 116023 (P. R. China)

Dr. D. Li
Institutes of Physics Science and Information Technology, Anhui University
Hefei, Anhui 230601 (P. R. China)

Dr. C. Ding
Dalian National Laboratory for Clean Energy, State Key Laboratory of Catalysis, Dalian Institute of Chemical Physics, Chinese Academy of Sciences
Dalian, Liaoning 116023 (P. R. China)

Supporting information and the ORCID identification number(s) for the author(s) of this article can be found under: https://doi.org/10.1002/anie.202011614.

ened migration path to reach the substrates that are diffused inside the pores, resulting in efficient e-h separation. In this context, metal-organic frameworks (MOFs),[8] a class of crystalline porous materials constructed by metal ions/clusters and organic ligands, have been recognized their great potential in photocatalysis.[9–11] Not limited to the advantages of porous solids mentioned above, the high crystallinity of MOFs has a positive effect on charge separation and photocatalysis, as the structural defects usually behave as recombination centers of e-h pairs. In fact, it has been well accepted that MOFs possess congenital capability to encapsulate small guest nanoparticles (NPs) for synergistic catalysis.[12] Therefore, MOF might be an ideal platform for incorporating small-size and highly dispersed TMP NPs for enhanced photocatalytic H_2 production.

With the aforementioned in mind, we have pre-synthesized tiny monodisperse TMPs (Ni_2P, $Ni_{12}P_5$) and Pt NPs in similar sizes ($\approx$10 nm) and assembled them into a representative MOF, UiO-66-NH_2 ($Zr_6O_4(OH)_4$(BDC-NH_2)$_6$, BDC-NH_2 = 2-amino-1,4-benzenedicarboxylic acid), to give the corresponding composites, denoted Ni_2P@UiO-66-NH_2, $Ni_{12}P_5$@UiO-66-NH_2 and Pt@UiO-66-NH_2, respectively (Scheme 1). Significantly, the TMPs greatly boost the photocatalytic H_2 production performance and Ni_2P NPs exhibit even higher H_2 production rate than Pt NPs. While energy level analysis and linear sweep voltammetry (LSV) reveal that Pt is thermodynamically favorable, Ni_2P is kinetically preferred, as supported by the photoelectrochemical measurements. The superior H_2 production of Ni_2P to Pt should be a balanced result between thermodynamics and dynamics. More importantly, by taking Ni_2P as a representative example, it is unambiguously demonstrated that Ni_2P behaves a similar role to Pt, accelerating the link-to-cluster charge transfer (LCCT) in photocatalytic process, based on electronic spin resonance (ESR) and ultrafast transient absorption (TA) spectroscopy, the latter of which presents similar real-time photoexcited carrier dynamics between Ni_2P and Pt. To our knowledge, in addition to the only report on the physical mixture of MOF and large sizes of TMPs toward photocatalysis,[6c] this is the first attempt on incorporating monodisperse and small TMPs into MOFs for photocatalysis.

Results and Discussion

The TMPs (e.g. Ni_2P, $Ni_{12}P_5$) with uniform sizes of $\approx$10 nm were synthesized in nitrogen atmosphere (Figure S1 in the Supporting Information, SI).[13] Their phase purity was confirmed based on powder X-ray diffraction (XRD) profiles (Figure S2). The obtained TMPs were dispersed in DMF with $ZrCl_4$ and 2-aminoterephthalic acid to afford Ni_2P@UiO-66-NH_2 and $Ni_{12}P_5$@UiO-66-NH_2 with good crystallinity, in a regular octahedral shape and $\approx$1 μm sizes (Figure S2 and S3). Upon encapsulation in the MOF, the TMPs remain to be $\approx$10.0 nm, in a uniformly dispersed form inside the MOF particles, as verified by transmission electron microscopy (TEM) observation (Figure 1 a,b and Figure S4).

For control experiments, Pt NPs with sizes of $\approx$10 nm were synthesized and Pt@UiO-66-NH_2 of $\approx$1 μm was fabricated with a similar method as above (Figure S1 and S3). The Pt NPs present good dispersion in the MOF particles (Figure 1 c,d and S5). Not limited to the particle sizes, the loading amount of the cocatalyst and the BET surface areas of all the three MOF composite photocatalysts are similar (Figure S6 and Table S1). All their UV-vis diffuse reflectance spectra inherit the feature of UiO-66-NH_2 and almost exhibit the same band gap, indicating their similar light harvesting behavior (Figure S7). All these important features make it fair for their activity comparison with a focus on their different cocatalysts, Ni_2P, $Ni_{12}P_5$ and Pt NPs. In addition, the lowest unoccupied molecular orbital (LUMO) level of UiO-66-NH_2, which has been estimated by Mott-Schottky mea-

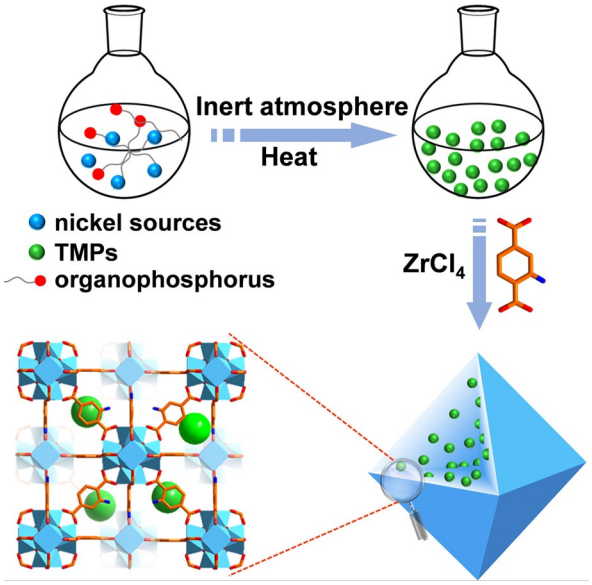

Scheme 1. Schematic illustration for the synthesis of TMPs and TMPs@UiO-66-NH_2.

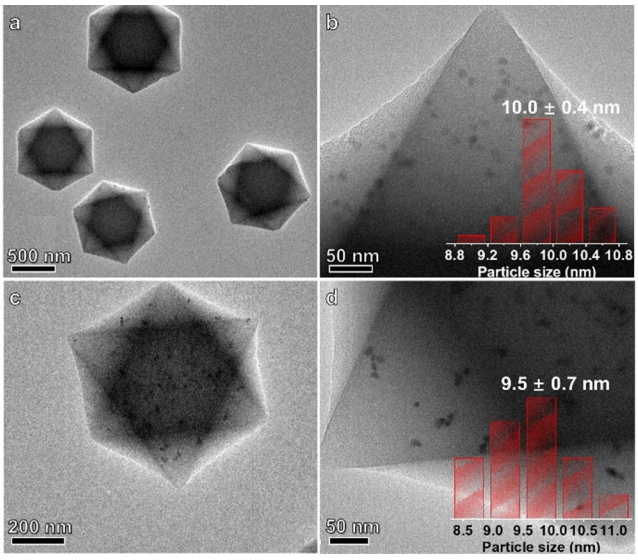

Figure 1. TEM images of a,b) Ni_2P@UiO-66-NH_2 (inset: size distribution of Ni_2P NPs) and c,d) Pt@UiO-66-NH_2 (inset: size distribution of Pt NPs).

surement (Figure 2a), is ≈ −0.62 V (vs. NHE, pH 6.8). This value is lower than the potential for H_2O reduction (−0.40 V vs. NHE, pH 6.8), suggesting its feasibility toward H_2 production.

Encouraged by the above information, photocatalytic H_2 production by water splitting was conducted under visible light irradiation. In stark contrast to the negligible H_2 production rate of pristine UiO-66-NH_2 (2.1 μmol g^{-1} h^{-1}), both TMPs@UiO-66-NH_2 exhibit exponential enhancement of photocatalytic activity. The $Ni_{12}P_5$@UiO-66-NH_2 shows H_2 production rate of 293.2 μmol g^{-1} h^{-1}, ≈80 times higher than the MOF. Strikingly, with the help of similar cocatalyst contents, Ni_2P@UiO-66-NH_2 and Pt@UiO-66-NH_2 possess over two orders of magnitude activity enhancement, 409.1 and 378.0 μmol g^{-1} h^{-1}, respectively (Figure 2b, S8 and Table S3), which are even tens of times higher than all physical mixtures of TMPs/Pt and UiO-66-NH_2 (Table S4). The results reflect the formation of TMP-MOF and Pt-MOF Schottky junction, where TMPs and Pt steer the rapid charge transfer from the MOF to the cocatalyst, suppressing e-h recombination and thereby achieving excellent efficiency of proton reduction. Further recycling experiments for Ni_2P@UiO-66-NH_2 suggest the well retained activity in the consecutive three catalytic runs (Figure 2c). Powder XRD, ICP and TEM results provide the evidences on its structural maintenance during the reaction (Figure S9 and S10).

It is well accepted that, for photocatalytic H_2 reduction in the presence of sacrificial agent, the law of reaction thermodynamics needs to be followed:[2]

$$E_{CB} > E_{H_2/H^+} + E_R \quad (1)$$

Where E_{CB} is the energy of conduction band (or LUMO) of the photocatalyst, E_{H_2/H^+} is the potential for H_2O reduction, and E_R is the overpotential for water reduction. Though UiO-66-NH_2 is theoretically able to give electrons for proton reduction as characterized above, its hydrogen production rate is very low. Introducing cocatalyst can significantly reduce E_R and improve the hydrogen production rate. The ability of a cocatalyst to lower E_R can be reflected by the on-set overpotential of the hydrogen evolution reaction (HER) process.[14] It is apparent that the on-set overpotential of Pt NPs is much lower than that of Ni_2P and $Ni_{12}P_5$ NPs (Figure 2d and S11), unambiguously demonstrating that Pt is thermodynamically superior to Ni_2P and $Ni_{12}P_5$. Meanwhile, the work function of Pt is larger, which means that the driving force of photo-generated electron transfer to Pt is greater.[3a,b] Therefore, from the perspective of thermodynamics, Pt is undoubtedly one of the best cocatalysts, which is consistent with the previous findings,[3] and the capability to accept electrons follows the order of Pt > Ni_2P > $Ni_{12}P_5$.

Following the thermodynamic principle, the activity of Pt@UiO-66-NH_2 should be much higher than the other two. Unexpectedly, Ni_2P@UiO-66-NH_2 has been confirmed to be more active. This result illustrates that the capability of accepting electrons is not the only criterion to evaluate a cocatalyst. The electron transfer kinetics between MOF and the cocatalyst should be taken into account as well. To this end, combined characterizations have been adopted. Steady-

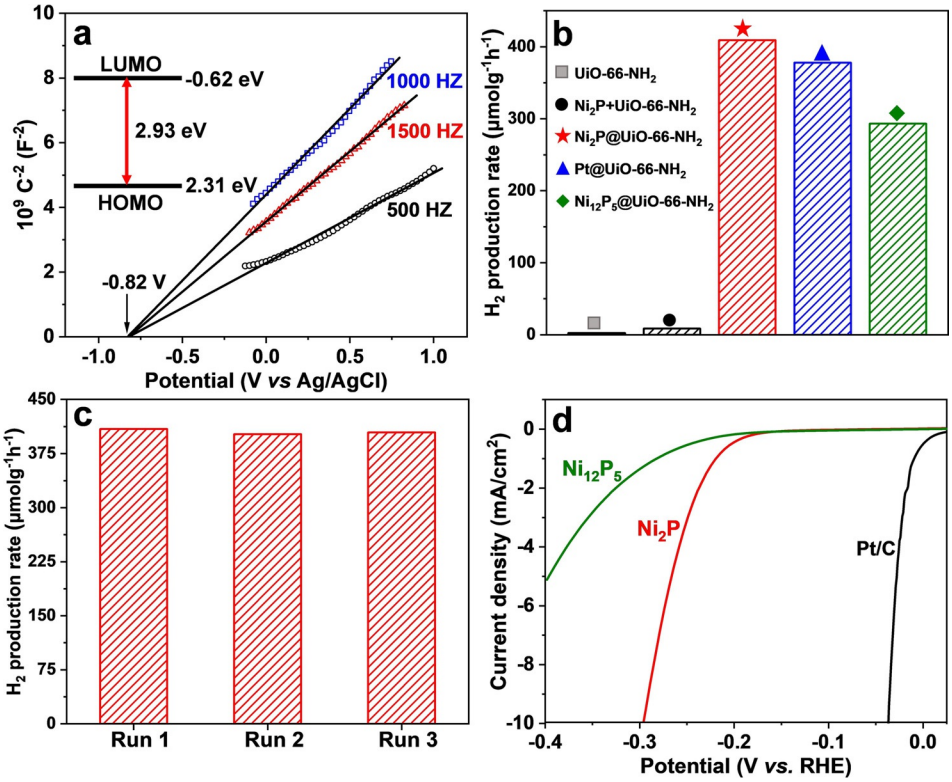

Figure 2. a) Mott-Schottky plots of UiO-66-NH_2 in 0.1 M Na_2SO_4 aqueous solution (pH 6.8) (inset: the energy diagram of UiO-66-NH_2). b) The photocatalytic hydrogen production rates of UiO-66-NH_2, physical mixture of Ni_2P and UiO-66-NH_2, Ni_2P@UiO-66-NH_2, Pt@UiO-66-NH_2 and $Ni_{12}P_5$@UiO-66-NH_2. c) Recycling performance of Ni_2P@UiO-66-NH_2. d) LSV curves of Ni_2P, $Ni_{12}P_5$ and Pt/C.

state photoluminescence (PL) spectra under excitation at 380 nm show that the MOF and all composites give a broad band centered at ≈450 nm, whereas the intensity is distinctly different and follows UiO-66-NH_2 > $Ni_{12}P_5$@UiO-66-NH_2 > Pt@UiO-66-NH_2 > Ni_2P@UiO-66-NH_2 (Figure 3a). The reduced intensity of PL signal in the composites in reference to the MOF reveals rapid electron transfer from the MOF to Pt and the most efficient electron transfer takes place in the Ni_2P composite. Photocurrent results disclose the e-h separation efficiency of photocatalysts and stay in line with the PL trend. As expected, the photocurrent of the parent MOF gets greatly enhanced after incorporating cocatalyst NPs, where Ni_2P@UiO-66-NH_2 exhibits the strongest photocurrent response, followed by Pt@UiO-66-NH_2, $Ni_{12}P_5$@UiO-66-NH_2 and UiO-66-NH_2 (Figure 3b), indicating the promoted separation of e-h pairs via the formation of MOF-cocatalyst Schottky junction and the best charge transfer in Ni_2P@UiO-66-NH_2 under light irradiation. This argument is also verified by electrochemical impedance spectroscopy (EIS) characterization (Figure 3c), in which all composites exhibit smaller radii than the parent MOF and Ni_2P@UiO-66-NH_2 presents the smallest radius, indicative of its lowest resistance of interfacial charge transfer. It is surprising that all kinetic data are miraculously consistent with the photocatalytic hydrogen production rate. Therefore, although Pt is easier to accept electrons from UiO-66-NH_2 than Ni_2P based on thermodynamic analysis, from the kinetic data and the photocatalytic results, we are able to reach the conclusion that the electrons migrate more efficiently from the MOF to Ni_2P than Pt, and followed by $Ni_{12}P_5$. By integrating thermodynamic and kinetic factors, it is ready to conclude that the overall trend of promoting charge separation capability is Ni_2P > Pt > $Ni_{12}P_5$, matching with the experimental results.

In order to further rationalize the results above, by taking Ni_2P and Pt as representative examples, mechanistic information from electron spin resonance (ESR) and ultrafast transient absorption (TA) spectroscopy has been gleaned. The Pt is recognized to accelerate the link-to-cluster charge transfer (LCCT) process in photocatalytic hydrogen production, where oxygen-centered active sites in Zr-oxo clusters can be generated.[15] To our delight, a new ESR signal at g_{iso} = 2.003 (close to the value of free electrons, g_e = 2.0023) emerges in all samples (Figure 3d). The much higher signal intensity is similarly observed in both Ni_2P@UiO-66-NH_2 and Pt@UiO-66-NH_2 than that in the parent MOF, which demonstrates the LCCT process and verifies the similar role of Ni_2P and Pt, being a cocatalyst. The differentiated intensity of ESR signal and photocatalytic activity can be ascribed to the different ability of the cocatalyst to accelerate LCCT process. Furthermore, ultrafast TA spectroscopy was resorted to track in real time the charge carrier dynamics for these photocatalysts. The TA spectra are similar whether or not a cocatalyst is introduced, indicating that the cocatalysts do not significantly affect the MOF light absorption, as also supported by UV-vis spectra (Figure S7). Compared with Pt@UiO-66-NH_2 and UiO-66-NH_2, Ni_2P@UiO-66-NH_2 exhibits a weaker stimulated emission (SE) signal (−) in the range of 420–530 nm when probed at the same delay times

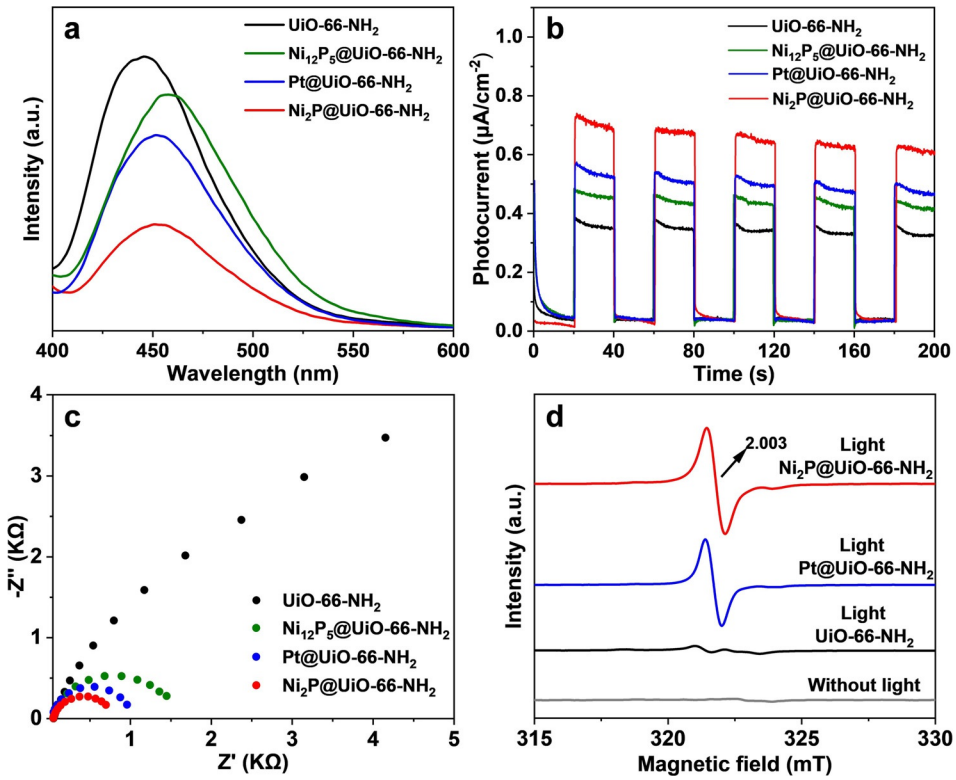

Figure 3. a) Photoluminescence (PL) emission spectra under excitation at 380 nm. b) Photocurrent responses. c) Electrochemical impedance spectroscopy (EIS) plots. d) Electronic spin resonance (ESR) spectra of UiO-66-NH_2 in dark and UiO-66-NH_2, Pt@UiO-66-NH_2 and Ni_2P@UiO-66-NH_2 under illumination.

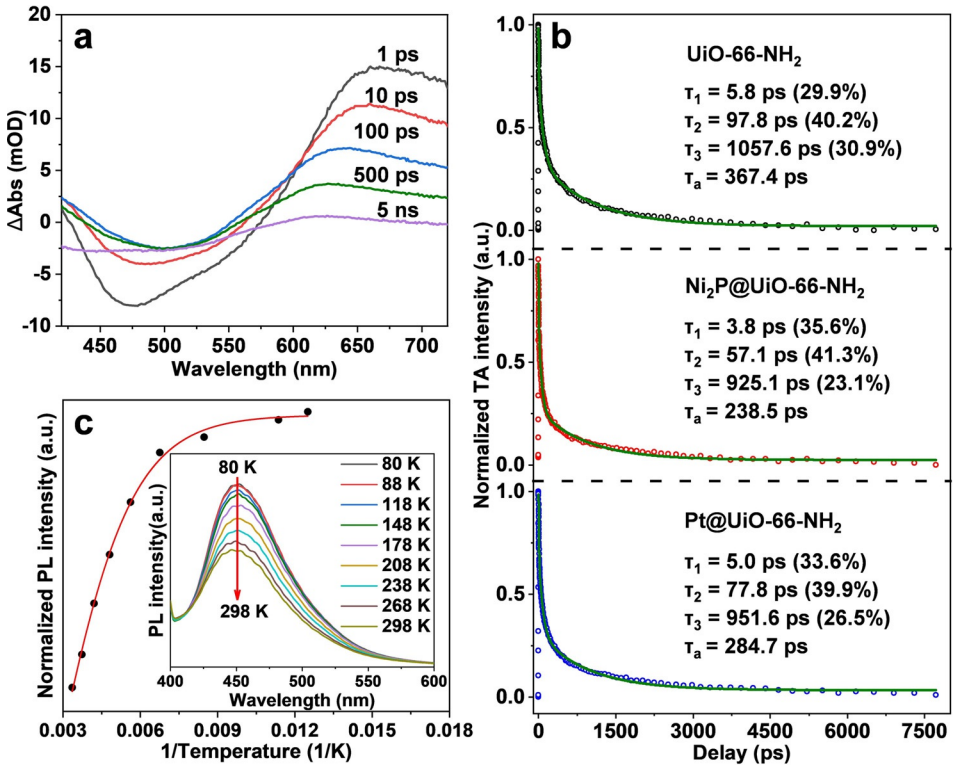

Figure 4. a) TA spectra of UiO-66-NH_2 (pump at 380 nm) taken at several representative probe delays. b) TA kinetics of UiO-66-NH_2, Ni_2P@UiO-66-NH_2 and Pt@UiO-66-NH_2 near 650 nm and their multi-exponential fits. c) The intensity of PL emission (λ_{ex} = 380 nm) as a function of temperature for Ni_2P@UiO-66-NH_2 (Inset: temperature-dependent PL spectra for Ni_2P@UiO-66-NH_2).

(Figure 4a and S12), indicative of efficient excited state quenching by Ni_2P. This is consistent with the PL intensities observed in Figure 3a, which also shows that Ni_2P quenches the PL of UiO-66-NH_2 more effectively than Pt. Moreover, there is a strong photoinduced absorptive peak at ≈650 nm that can be observed for Ni_2P and Pt loaded UiO-66-NH_2 but not for pure UiO-66-NH_2, suggesting that this feature is likely an indication of excited state charge transfer from UiO-66-NH_2 to cocatalysts.[16]

To further unveil the excited state dynamics of these photocatalysts, their TA kinetics of excited state absorption (ESA) at 650 nm are compared (Figure S13). All kinetics traces can be fitted by a three-exponential decay function (fitting parameters in Table S2) (Figure 4b). The average relaxation lifetime is 367.4, 238.5 and 284.7 ps for UiO-66-NH_2, Ni_2P@UiO-66-NH_2 and Pt@UiO-66-NH_2, respectively. Accurate assignment of these multiple time constants is challenging as they could arise from charge transfer, various trapping processes and/or intrinsic lifetime heterogeneities. Nonetheless, the facts that the average relaxation lifetime of Ni_2P@UiO-66-NH_2 is shorter than Pt@UiO-66-NH_2 and that both are shorter than pure UiO-66-NH indicate that charge transfer from UiO-66-NH_2 to Ni_2P is more efficient than to Pt, again consistent with the higher photocatalytic activity of Ni_2P@UiO-66-NH_2.[16,17]

In addition, apparent activation energy (E_a), an important parameter combining thermodynamic and dynamic factors to reflect the difficulty of a reaction, can be evaluated based on the temperature-dependent PL spectra. With the temperature increasing, the PL peak intensity gradually decreases (Figure 4c and S14), and the E_a can be estimated by the following Arrhenius equation:[18]

$$I(T) = I_o/(1 + A\exp(-E_a/k_B T)) \quad (2)$$

According to the equation, the E_a values of UiO-66-NH_2, Pt@UiO-66-NH_2 and Ni_2P@UiO-66-NH_2 are 69.2, 66.3 and 57.7 meV, respectively. The change trend of E_a is exactly opposite to that of hydrogen production rate (Figure 4c and S15). This result, once again, suggests that the cocatalysts reduce the reaction energy barrier and boost the reaction activity. The lower E_a of Ni_2P@UiO-66-NH_2 nicely supports its better performance than Pt@UiO-66-NH_2 in our system.

Conclusion

In this work, small-size and monodisperse NPs of TMPs, for the first time, have been rationally incorporated into a MOF for photocatalysis. For control, Pt NPs have also been assembled into the MOF particle. Both TMPs and Pt have been demonstrated to be the similar role of cocatalyst to accept the electrons and promote the charge transfer. The electron-injected TMPs and Pt encompassed by the MOF are easily accessible to protons for photocatalytic H_2 production. As a result, the activity of Ni_2P@UiO-66-NH_2 outperforms all other counterparts, even Pt@UiO-66-NH_2, unambiguously demonstrating that this is an integrated performance between

thermodynamic and kinetic results, though the Pt possesses much more favorable thermodynamics than TMPs. As expected, a series of photoelectrochemical and spectroscopic observations elucidate the underlying electron-transfer mechanism and manifest the faster kinetics and more efficient charge separation in Ni_2P@UiO-66-NH_2 than Pt@UiO-66-NH_2 and others. We believe this work will not only enable in-depth understanding on the charge transfer in MOF composites, but also provide inspirations for building efficient and noble-metal-free MOF-based and even other porous material-based photocatalytic systems.

Acknowledgements

This work was supported by the National Natural Science Foundation of China (21725101, 21673213 and 21521001) and the DNL Cooperation Fund, Chinese Academy of Sciences (DNL201911).

Conflict of interest

The authors declare no conflict of interest.

Keywords: cocatalysts · hydrogen production · metal-organic frameworks · photocatalysis · transition-metal phosphides

[1] a) Z. Han, R. Eisenberg, *Acc. Chem. Res.* **2014**, *47*, 2537 – 2544; b) J. H. Kim, D. Hansora, P. Sharma, J. W. Jang, J. S. Lee, *Chem. Soc. Rev.* **2019**, *48*, 1908 – 1971; c) B. Zhang, L. Sun, *Chem. Soc. Rev.* **2019**, *48*, 2216 – 2264.

[2] a) X. Chen, S. Shen, L. Guo, S. S. Mao, *Chem. Rev.* **2010**, *110*, 6503 – 6570; b) X. Meng, L. Liu, S. Ouyang, H. Xu, D. Wang, N. Zhao, J. Ye, *Adv. Mater.* **2016**, *28*, 6781 – 6803; c) Y. Wang, A. Vogel, M. Sachs, R. S. Sprick, L. Wilbraham, S. J. A. Moniz, R. Godin, M. A. Zwijnenburg, J. R. Durrant, A. I. Cooper, J. Tang, *Nat. Energy* **2019**, *4*, 746 – 760; d) Z. Wang, C. Li, K. Domen, *Chem. Soc. Rev.* **2019**, *48*, 2109 – 2125.

[3] a) J. Yang, D. Wang, H. Han, C. Li, *Acc. Chem. Res.* **2013**, *46*, 1900 – 1909; b) J. Ran, M. Jaroniec, S. Z. Qiao, *Adv. Mater.* **2018**, *30*, 1704649; c) A. Y. Meng, L. Y. Zhang, B. Cheng, J. G. Yu, *Adv. Mater.* **2019**, *31*, 1807660.

[4] a) J. F. Callejas, J. M. McEnaney, C. G. Read, J. C. Crompton, A. J. Biacchi, E. J. Popczun, T. R. Gordon, N. S. Lewis, R. E. Schaak, *ACS Nano* **2014**, *8*, 11101 – 11107; b) S. Cao, Y. Chen, C. J. Wang, X. J. Lv, W. F. Fu, *Chem. Commun.* **2015**, *51*, 8708 – 8711; c) Y. Shi, B. Zhang, *Chem. Soc. Rev.* **2016**, *45*, 1529 – 1541; d) J. Zhang, W. Yao, C. Huang, P. Shi, Q. Xu, *J. Mater. Chem. A* **2017**, *5*, 12513 – 12519; e) Z. Sun, M. Zhu, X. Lv, Y. Liu, C. Shi, Y. Dai, A. Wang, T. Majima, *Appl. Catal. B* **2019**, *246*, 330 – 336.

[5] P. Liu, J. A. Rodriguez, *J. Am. Chem. Soc.* **2005**, *127*, 14871 – 14878.

[6] a) Z. Sun, H. Zheng, J. Li, P. Du, *Energy Environ. Sci.* **2015**, *8*, 2668 – 2676; b) A. Indra, A. Acharjya, P. W. Menezes, C. Merschjann, D. Hollmann, M. Schwarze, M. Aktas, A. Friedrich, S. Lochbrunner, A. Thomas, M. Driess, *Angew. Chem. Int. Ed.* **2017**, *56*, 1653 – 1657; *Angew. Chem.* **2017**, *129*, 1675 – 1679; c) S. Kampouri, T. N. Nguyen, C. P. Ireland, B. Valizadeh, F. M. Ebrahim, G. Capano, D. Ongari, A. Mace, N. Guijarro, K. Sivula, A. Sienkiewicz, L. Forró, B. Smit, K. C. Stylianou, *J. Mater. Chem. A* **2018**, *6*, 2476 – 2481; d) W. Bi, L. Zhang, Z. Sun, X. Li, T. Jin, X. Wu, Q. Zhang, Y. Luo, C. Wu, Y. Xie, *ACS Catal.* **2016**, *6*, 4253 – 4257.

[7] a) W. Zhou, W. Li, J. Q. Wang, Y. Qu, Y. Yang, Y. Xie, K. Zhang, L. Wang, H. Fu, D. Zhao, *J. Am. Chem. Soc.* **2014**, *136*, 9280 – 9283; b) T. Zhang, W. Lin, *Chem. Soc. Rev.* **2014**, *43*, 5982 – 5993; c) V. S. Vyas, F. Haase, L. Stegbauer, G. Savasci, F. Podjaski, C. Ochsenfeld, B. V. Lotsch, *Nat. Commun.* **2015**, *6*, 8508; d) Q. Lin, X. Bu, C. Mao, X. Zhao, K. Sasan, P. Feng, *J. Am. Chem. Soc.* **2015**, *137*, 6184 – 6187; e) J. D. Xiao, H.-L. Jiang, *Acc. Chem. Res.* **2019**, *52*, 356 – 366.

[8] a) H. Furukawa, K. E. Cordova, M. O'Keeffe, O. M. Yaghi, *Science* **2013**, *341*, 1230444; b) H. C. Zhou, S. Kitagawa, *Chem. Soc. Rev.* **2014**, *43*, 5415 – 5418; c) B. Li, H. M. Wen, Y. Cui, W. Zhou, G. Qian, B. Chen, *Adv. Mater.* **2016**, *28*, 8819 – 8860; d) T. Islamoglu, S. Goswami, Z. Li, A. J. Howarth, O. K. Farha, J. T. Hupp, *Acc. Chem. Res.* **2017**, *50*, 805 – 813.

[9] a) A. Fateeva, P. A. Chater, C. P. Ireland, A. A. Tahir, Y. Z. Khimyak, P. V. Wiper, J. R. Darwent, M. J. Rosseinsky, *Angew. Chem. Int. Ed.* **2012**, *51*, 7440 – 7444; *Angew. Chem.* **2012**, *124*, 7558 – 7562; b) S. Pullen, H. Fei, A. Orthaber, S. M. Cohen, S. Ott, *J. Am. Chem. Soc.* **2013**, *135*, 16997 – 17003; c) T. Zhou, Y. Du, A. Borgna, J. Hong, Y. Wang, J. Han, W. Zhang, R. Xu, *Energy Environ. Sci.* **2013**, *6*, 3229 – 3234; d) X. Y. Dong, M. Zhang, R. B. Pei, Q. Wang, D. H. Wei, S. Q. Zang, Y. T. Fan, T. C. Mak, *Angew. Chem. Int. Ed.* **2016**, *55*, 2073 – 2077; *Angew. Chem.* **2016**, *128*, 2113 – 2117; e) Y. An, Y. Liu, P. An, J. Dong, B. Xu, Y. Dai, X. Qin, X. Zhang, M. H. Whangbo, B. Huang, *Angew. Chem. Int. Ed.* **2017**, *56*, 3036 – 3040; *Angew. Chem.* **2017**, *129*, 3082 – 3086; f) Q. Zuo, T. Liu, C. Chen, Y. Ji, X. Gong, Y. Mai, Y. Zhou, *Angew. Chem. Int. Ed.* **2019**, *58*, 10198 – 10203; *Angew. Chem.* **2019**, *131*, 10304 – 10309.

[10] a) Y. Fu, D. Sun, Y. Chen, R. Huang, Z. Ding, X. Fu, Z. Li, *Angew. Chem. Int. Ed.* **2012**, *51*, 3364 – 3367; *Angew. Chem.* **2012**, *124*, 3420 – 3423; b) S. Wang, W. Yao, J. Lin, Z. Ding, X. Wang, *Angew. Chem. Int. Ed.* **2014**, *53*, 1034 – 1038; *Angew. Chem.* **2014**, *126*, 1052 – 1056; c) H. Q. Xu, J. Hu, D. Wang, Z. Li, Q. Zhang, Y. Luo, S. H. Yu, H.-L. Jiang, *J. Am. Chem. Soc.* **2015**, *137*, 13440 – 13443; d) H. Zhang, J. Wei, J. Dong, G. Liu, L. Shi, P. An, G. Zhao, J. Kong, X. Wang, X. Meng, J. Zhang, J. Ye, *Angew. Chem. Int. Ed.* **2016**, *55*, 14310 – 14314; *Angew. Chem.* **2016**, *128*, 14522 – 14526; e) Y. Wang, N. Y. Huang, J. Q. Shen, P. Q. Liao, X. M. Chen, J. P. Zhang, *J. Am. Chem. Soc.* **2018**, *140*, 38 – 41; f) E. X. Chen, M. Qiu, Y. F. Zhang, Y. S. Zhu, L. Y. Liu, Y. Y. Sun, X. H. Bu, J. Zhang, Q. P. Lin, *Adv. Mater.* **2018**, *30*, 1704388; g) L. Z. Dong, L. Zhang, J. Liu, Q. Huang, M. Lu, W. X. Ji, Y. Q. Lan, *Angew. Chem. Int. Ed.* **2020**, *59*, 2659 – 2663; *Angew. Chem.* **2020**, *132*, 2681 – 2685.

[11] a) K. G. Laurier, F. Vermoortele, R. Ameloot, D. E. De Vos, J. Hofkens, M. B. Roeffaers, *J. Am. Chem. Soc.* **2013**, *135*, 14488 – 14491; b) L. Shen, M. Luo, L. Huang, P. Feng, L. Wu, *Inorg. Chem.* **2015**, *54*, 1191 – 1193; c) J.-D. Xiao, Q. Shang, Y. Xiong, Q. Zhang, Y. Luo, S.-H. Yu, H.-L. Jiang, *Angew. Chem. Int. Ed.* **2016**, *55*, 9389 – 9393; *Angew. Chem.* **2016**, *128*, 9535 – 9539; d) J. Ran, J. Qu, J. Zhang, H. Wen, T. Wang, H. Chen, S. Zhang, L. Song, X. Zhang, L. Jing, R. Zheng, S. Z. Qiao, *Adv. Energy Mater.* **2019**, *9*, 1803402.

[12] a) Q. L. Zhu, Q. Xu, *Chem. Soc. Rev.* **2014**, *43*, 5468 – 5512; b) A. Dhakshinamoorthy, A. M. Asiri, H. Garcia, *ACS Catal.* **2017**, *7*, 2896 – 2919; c) Q. Yang, Q. Xu, H.-L. Jiang, *Chem. Soc. Rev.* **2017**, *46*, 4774 – 4808; d) G. Li, S. Zhao, Y. Zhang, Z. Tang, *Adv. Mater.* **2018**, *30*, 1800702; e) L. Y. Wu, Y. F. Mu, X. X. Guo, W. Zhang, Z. M. Zhang, M. Zhang, T. B. Lu, *Angew. Chem. Int. Ed.* **2019**, *58*, 9491 – 9495; *Angew. Chem.* **2019**, *131*, 9591 – 9595.

[13] a) E. J. Popczun, J. R. McKone, C. G. Read, A. J. Biacchi, A. M. Wiltrout, N. S. Lewis, R. E. Schaak, *J. Am. Chem. Soc.* **2013**, *135*,

9267 – 9270; b) Z. Huang, Z. Chen, Z. Chen, C. Lv, H. Meng, C. Zhang, *ACS Nano* **2014**, *8*, 8121 – 8129.
[14] a) D. Wang, R. Li, J. Zhu, J. Shi, J. Han, X. Zong, C. Li, *J. Phys. Chem. C* **2012**, *116*, 5082 – 5089; b) W. Zhen, J. Ma, G. Lu, *Appl. Catal. B* **2016**, *190*, 12 – 25; c) Q. Wang, T. Hisatomi, Y. Suzuk, Z. Pan, J. Seo, M. Katayama, T. Minegishi, H. Nishiyama, T. Takata, K. Seki, A. Kudo, T. Yamada, K. Domen, *J. Am. Chem. Soc.* **2017**, *139*, 1675 – 1683.
[15] H. Liu, C. Xu, D. Li, H.-L. Jiang, *Angew. Chem. Int. Ed.* **2018**, *57*, 5379 – 5383; *Angew. Chem.* **2018**, *130*, 5477 – 5481.
[16] S. Z. Yang, W. H. Hu, X. Zhang, P. L. He, B. Pattengale, C. M. Liu, M. Cendejas, I. Hermans, X. Y. Zhang, J. Zhang, J. Huang, *J. Am. Chem. Soc.* **2018**, *140*, 14614 – 14618.
[17] X. Fan, J. Wang, K. Wu, L. Zhang, J. Zhang, *Angew. Chem. Int. Ed.* **2019**, *58*, 1320 – 1323; *Angew. Chem.* **2019**, *131*, 1334 – 1337.
[18] P. Yu, X. Wen, Y.-R. Toh, J. Tang, *J. Phys. Chem. C* **2012**, *116*, 6567 – 6571.

Manuscript received: August 25, 2020
Accepted manuscript online: September 8, 2020
Version of record online: October 6, 2020

